Many-particle nucleon-nucleon forces from nuclear single-particle states

B.L. Birbrair*and V.I. Ryazanov
Petersburg Nuclear Physics Institute
Gatchina, St.Petersburg 188350, Russia

Abstract

As follows from the energies of single-particle states in ^{40}Ca, ^{90}Zr and ^{208}Pb nuclei the contribution of many-particle NN forces to the nuclear single-particle potential is at least the sum of repulsive and attractive parts resulting from three-particle and four-particle forces respectively. In addition the specified nucleon density distributions in the above nuclei are determined from both the 1 GeV proton-nucleus elastic scattering and the single-particle energies.

1 Introduction

The nucleon-nucleon interaction proceeds via the meson exchange, and therefore the existence of many-particle NN forces is a natural consequence of nonlinearity of the strong interaction theory. Indeed, only two-particle forces, Fig.1a, are possible in the lowest order of linear theory containing only quadratic terms of the meson field φ in the meson Lagrangian density. The situation is different in nonlinear theories. In the theory with φ^3 terms the meson may turn into two ones thus giving rise to three-particle forces, Fig.1b, in addition to the pairing ones. In the same way the lowest-order four-particle forces, Fig.1c, appear in the theory with φ^4 terms. No higher-power terms exist in renormalizable theories, but the branching of meson is possible in higher orders thus giving rise to higher NN forces, Fig.1d. For this reason the empirical information on many-particle forces is of fundamental importance for the physics of strong interactions.

At present the only such information is provided by the calculations for the few-nucleon systems. According to these calculations something should be added to the two-particle NN forces to get the agreement between the calculated and observed quantities. In practice only three-particle forces are added (see Ref.[1] and the references therein) since the problem is difficult even in this case. Indeed, the forces are characterized by a number of adjustable parameters describing the strength, range, the spin-isospin structure etc.,

*Birbrair@thd.pnpi.spb.ru

and the observed quantities are expressed through these parameters in all orders of the perturbation theory. In such conditions it is hardly possible to distinguish, for instance, between the genuine three-particle interaction and the combination of the latter with the four-particle one.

As shown in the present paper such possibility may be provided by the experimental data on nuclear single-particle states. It is based on the facts that (a) the contribution of the two-particle NN forces to the nuclear single-particle potential is fixed by experiment and (b) no correlation effects contribute to the single-particle energies [2]. For these reasons the many-particle contribution may be detected by comparing the observed energies of single-particle states with the calculations including the two-particle NN forces only.

2 Nuclear single-particle states

We are using the untraditional approach by M.Baranger [2]. It is based on the spectral representation for the single-particle propagator [3, 4]

$$\begin{aligned} & S_A(x,x';\tau) \;=\; -i\langle A_0|T\psi(x,\tau)\psi^+(x',0)|A_0\rangle \\ = \quad & i\theta(-\tau)\sum_j \psi_j(x)\psi_j^+(x')e^{-iE_j\tau} - i\theta(\tau)\sum_k \psi_k(x)\psi_k^+(x')e^{-iE_k\tau}\ , \end{aligned} \tag{1}$$

where $|A_0\rangle$ is the ground-state wave function of nucleus A which is chosen to be even-even the ground state thus being nondegenerate,

$$\begin{aligned} \psi_j(x) \;&=\; \langle (A-1)_j|\psi(x)|A_0\rangle\ , \quad E_j = \; \mathcal{E}_0(A) - \mathcal{E}_j(A-1) \\ \psi_k(x) \;&=\; \langle A_0|\psi(x)|(A+1)_k\rangle\ , \quad E_k = \; \mathcal{E}_k(A+1) - \mathcal{E}_0(A) \end{aligned} \tag{2}$$

the sums over j and k thus running over complete sets of states of $A-1$ and $A+1$ nuclei. The short-time behaviour of a particle or hole which is suddenly created in the ground state $|A_0\rangle$ is described by the following relations

$$\sum_j \psi_j(x)\psi_j^+(x') + \sum_k \psi_k(x)\psi_k^+(x') = i\Big(S_A(x,x';+0) - S_A(x,x';-0)\Big)$$

$$= \quad \delta(x-x') \tag{3}$$

$$\sum_j E_j\psi_j(x)\psi_j^+(x') + \sum_k E_k\psi_k(x)\psi_k^+(x') = -\Big(\dot{S}_A(x,x';+0) - \dot{S}_A(x,x';-0)\Big)$$

$$= \quad H_{sp}(x,x') \tag{4}$$

$$\sum_j E_j^2\psi_j(x)\psi_j^+(x') + \sum_k E_k^2\psi_k(x)\psi_k^+(x') = -i\Big(\ddot{S}_A(x,x';+0) - \ddot{S}_A(x,x';-0)\Big)$$

$$= \quad H_{sp}^2(x,x') + \Pi(x,x')\ , \tag{5}$$

where $\dot{S} = \partial S/\partial\tau$, $\ddot{S} = \partial^2 S/\partial\tau^2$. The single-particle states are treated as eigenstates of the single-particle Hamiltonian $H_{sp}(x,x')$, Eq.(4),

$$\varepsilon_\lambda\psi_\lambda(x) \;=\; \int H_{sp}(x,x')\psi_\lambda(x')dx' \tag{6}$$

thus being the doorway states for the single-nucleon transfer reactions[2]. As a result of the correlation effects these states are distributed over actual states of both the $A-1$ and $A+1$ nuclei. However the properties of the distribution process permit the determination of the single-particle energies from the experimental data. Introducing the spectroscopic factors

$$s_{j,k}^{(\lambda)} \;=\; \left| \int \psi_\lambda^+(x)\psi_{j,k}(x)dx \right|^2 \;, \tag{7}$$

multiplying Eqs. (3)–(5) by $\psi_\lambda^+(x)\psi_\lambda(x')$ and integrating over x and x' we get

$$\sum_j s_j^{(\lambda)} + \sum_k s_k^{(\lambda)} \;=\; 1 \tag{3a}$$

$$\sum_j E_j s_j^{(\lambda)} + \sum_k E_k s_k^{(\lambda)} \;=\; \varepsilon_\lambda \tag{4a}$$

$$\sum_j E_j^2 s_j^{(\lambda)} + \sum_k E_k^2 s_k^{(\lambda)} \;=\; \varepsilon_\lambda^2 + \sigma_\lambda^2 \tag{5a}$$

$$\sigma_\lambda^2 \;=\; \int \psi_\lambda^+(x)\Pi(x,x')\psi_\lambda(x')dxdx' \;. \tag{8}$$

The determination of single-particle energies by using the Eqs. (3a)–(5a) and (8) will be discussed in Subsect.3.2.

The Ref.[2] derivation of the explicit form of the single-particle Hamiltonian H_{sp} should be specified by taking into account the meson-exchange nature of the NN interaction.

First, the contemporary meson-exchange forces such as the OBE [5], Paris [6] and Bonn [7] have no hard repulsive core, and therefore the problem of elimination of short-range correlations (see the discussion in Ref.[2]) does not really exist. So there are no actual reasons preventing from a direct use of bare NN forces for nuclear structure calculations (i.e. the preliminary calculation of the Brueckner G-matrix [8] or some different way of the hard core elimination is not necessary).

Second, the commutator technique of Ref.[2] does not apply in this case because of the retardation. For this reason the field-theoretical approach [3, 4] should be used instead. In this approach the single-particle Green function

$$G_A(x,x';\varepsilon) \;=\; \int S_A(x,x';\tau)\; e^{i\varepsilon\tau}\; d\tau \tag{9}$$

obeys the Dyson equation

$$\varepsilon G_A(x,x';\varepsilon) \;=\; \delta(x-x') + \hat{k}_x G_A(x,x';\varepsilon) + \int M(x,x_1;\varepsilon)G_A(x_1,x';\varepsilon)\; dx_1 \;, \tag{10}$$

where $\hat{k}_x$ is the kinetic energy and the mass operator $M(x,x';\varepsilon)$ consists of the energy-independent part $U(x,x')$, which is just the nuclear single-particle potential, and the energy-dependent one $\Sigma(x,x';\varepsilon)$ which is responsible for the correlation effects:

$$M(x,x';\varepsilon) \;=\; U(x,x') + \Sigma(x,x';\varepsilon) \;. \tag{11}$$

As shown in Refs.[4, 9] the quantity $\Sigma(x,x';\varepsilon)$ vanishes in the $\varepsilon\to\infty$ limit

$$\Sigma(x,x';\varepsilon) \;=\; \frac{\Pi(x,x')}{\varepsilon}+\cdots \tag{12}$$

(the dots in the rhs are the higher-power terms of ε^{-1}) and therefore

$$U(x,x') \;=\; \lim_{\varepsilon\to\infty}\; M(x,x';\varepsilon) \tag{13}$$

the decomposition (11) thus being unambiguous.

Let us show that the single-particle Hamiltonian of Eq.(4) is

$$H_{sp}(x,x') \;=\; \hat{k}_x\delta(x-x')+U(x,x')\;, \tag{14}$$

whereas the quantity $\Pi(x,x')$ of Eq.(5) is defined by Eq.(12). First let us note that according to the time-energy Heisenberg relation the infinite ε value is equivalent to the infinitely short time interval, the Eqs.(13) and (14) thus meaning that the Hamiltonian H_{sp} is indeed responsible for the short-time behaviour of the particle (hole).

Now let us use the spectral representation [3, 4]

$$G_A(x,x';\varepsilon) \;=\; \sum_j \frac{\psi_j(x)\psi_j^+(x')}{\varepsilon-E_j-i\delta}+\sum_k \frac{\psi_k(x)\psi_k^+(x')}{\varepsilon-E_k+i\delta} \tag{15}$$

and the identity

$$\frac{1}{\varepsilon-E} \;=\; \frac{1}{\varepsilon(1-E/\varepsilon)} \;=\; \frac{1}{\varepsilon}+\frac{E}{\varepsilon^2}+\frac{E^2}{\varepsilon^3}+\;\cdots \tag{16}$$

in the $\varepsilon\to\infty$ limit. Putting Eq.(16) into Eq.(15) we get the following asymptotic expansion

$$G_A(x,x';\varepsilon) \;=\; \frac{I_0(x,x')}{\varepsilon}+\frac{I_1(x,x')}{\varepsilon^2}+\frac{I_2(x,x')}{\varepsilon^3}+\;\cdots \tag{17}$$

the quantities $I_0(x,x'), I_1(x,x')$ and $I_2(x,x')$ being just the lhs of Eqs. (3),(4) and (5) respectively. As seen from Eqs.(11),(12) and (14) the Dyson equation (10) may be written in the form

$$\varepsilon G_A(x,x';\varepsilon) \;=\; \delta(x-x')+\int\left(H_{sp}(x,x_1)+\frac{\Pi(x,x_1)}{\varepsilon}+\cdots\right)G_A(x_1,x';\varepsilon)dx_1\;. \tag{18}$$

Putting Eq.(17) into Eq.(18) we again get Eqs.(3)–(5), but now the quantities H_{sp} and Π are determined.

In terms of bare NN forces (for a moment let us take into account the pairing forces only) the single-particle potential is defined by the first-order diagrams of Fig.2 provided the nucleons interact without the retardation [9]. This is however not the case for the meson-exchange forces including both the momentum and the energy transfer. As a result of the latter the exchange diagrams of Fig.2b have the ε^{-1} asymptotics thus contributing

to the quantity $\Sigma(x,x';\varepsilon)$ rather than $U(x,x')$ [10]. Let us illustrate this for the Bonn B potential [7]. It is the sum of the terms

$$v(q,\omega) \;=\; g^2\left(\frac{\Lambda^2-\mu^2}{\Lambda^2+q^2-\omega^2}\right)^{2\alpha}\;\frac{1}{\mu^2-q^2-\omega^2} \tag{19}$$

in the four-momentum space, the form of the meson-nucleon vertices being specified by the Lorentz symmetry of the mesons. The latter is however disregarded because it is irrelevant for the energy dependence. With this remark the expression for the Fig.2b diagram becomes

$$M_e(x,x';\varepsilon) \;=\; \int\frac{d^3\mathbf{q}}{(2\pi)^3}\;e^{i\mathbf{q}(\mathbf{r}-\mathbf{r}')}\int\frac{id\omega}{2\pi}\;v(q,\omega)G_A(x,x';\varepsilon+\omega)\;. \tag{20}$$

Considering the case of the monopole formfactor, $\alpha=1$, and using the identity

$$\begin{aligned}\left(\frac{\Lambda^2-\mu^2}{\Lambda^2+q^2-\omega^2}\right)^2\frac{1}{\mu^2+q^2-\omega^2} \;&=\; -\lim_{\delta\to 0}\left\{\frac{1}{2\omega_\mu(q)}\left(\frac{1}{\omega-\omega_\mu(q)+i\delta}-\frac{1}{\omega+\omega_\mu(q)-i\delta}\right)\right.\\ -\;&\left.\left(1-(\Lambda^2-\mu^2)\frac{\partial}{\partial\Lambda^2}\right)\frac{1}{2\omega_\Lambda(q)}\left(\frac{1}{\omega-\omega_\Lambda(q)+i\delta}-\frac{1}{\omega+\omega_\Lambda(q)-i\delta}\right)\right\}\;,\\ &\omega_\mu(q)=(\mu^2+q^2)^{1/2}\;,\quad \omega_\Lambda(q)=(\Lambda^2+q^2)^{1/2}\end{aligned} \tag{21}$$

we get

$$\begin{aligned}M_e(x,x';\varepsilon)=g^2\int\frac{d^3\mathbf{q}}{(2\pi)^3}e^{i\mathbf{q}(\mathbf{r}-\mathbf{r}')}\left\{\frac{1}{2\omega_\mu(q)}\left[\sum_j\frac{\psi_j(x)\psi_j^+(x')}{\varepsilon-E_j+\omega_\mu(q)}+\sum_k\frac{\psi_k(x)\psi_k^+(x')}{\varepsilon-E_k-\omega_\mu(q)}\right]\right.\\ \left.-\left(1-(\Lambda^2-\mu^2)\frac{\partial}{\partial\Lambda^2(q)}\right)\frac{1}{2\omega_\Lambda(q)}\left[\sum_j\frac{\psi_j(x)\psi_j^+(x')}{\varepsilon-E_j+\omega_\Lambda(q)}+\sum_k\frac{\psi_k(x)\psi_k^+(x')}{\varepsilon-E_k-\omega_\Lambda(q)}\right]\right\}.\end{aligned} \tag{22}$$

The sign is also irrelevant because the Bonn B potential is the sum of terms with different signs. In the $\varepsilon\to\infty$ limit we get

$$M_e(x,x';\varepsilon) \;=\; \frac{g^2}{4\pi^2}\frac{\delta(x-x')}{\varepsilon}\int\limits_0^\infty q^2\left[\frac{1}{\omega_\mu(q)}-\frac{1}{\omega_\Lambda(q)}-\frac{\Lambda^2-\mu^2}{2\omega_\Lambda^3(q)}\right]dq\;. \tag{23}$$

The integral is convergent because the integrand has the q^{-3} asymptotics. In addition to Fig.2b the quantity $\Sigma(x,x';\varepsilon)$ includes an infinite sum of higher-order Feynman diagrams describing all kinds of the correlation effects (Pauli, particle–particle, particle–hole, ground–state etc.).

Thus the only contribution to the nuclear single-particle potential is provided by the Hartree diagrams of Fig.2a and the Hartree-like ones of Fig.3 resulting from the many-particle NN forces, the single-particle energies thus being free of the correlation effects. The latter is the feature of the Ref.[2] approach, thus permitting the model-independent studies of nuclear structure.

3 Results

3.1 Single-particle potential

The Fig.2a contribution to the single-particle potential is the convolution of the two-particle NN forces with the nucleon density distribution in nucleus. The latter is determined by the combined analysis of electron-nucleus and 1 GeV proton-nucleus elastic scattering data [11]. The two-particle forces are determined from the deuteron properties and the elastic NN scattering phase shifts at the energies below the pion production threshold. In this way the "pairing" contribution to nuclear single-particle potential is fixed by the experimental data thus being independent of any nuclear model.

We have chosen the Bonn B potential [7] for the two-particle forces, the motivation being discussed in Sect.4. This choice enables us to check the status of nuclear relativity [12] by calculating the scalar and vector fields in nuclear interior. Using the parameters of Table 5 from Ref.[7] and the equilibrium nuclear matter density value $\rho_{eq} = 0.17$ fm^{-3} we get [10]

$$V \ = \ +284 \text{ MeV} , \qquad S \ = \ -367 \text{ MeV} . \tag{24}$$

These values are close to those provided by the Dirac phenomenology [13]. In such conditions it is reasonable to treat the single-particle wave functions $\psi_\lambda(x)$ as Dirac bispinors obeying the Dirac equation. The single-particle Hamiltonian resulting from the Bonn B potential is [10]

$$H_{sp} = \ -i\gamma^0\boldsymbol{\gamma}\boldsymbol{\nabla} + i\Phi(r)\ \boldsymbol{\gamma}\frac{\mathbf{r}}{r} + (\gamma^0 - 1)m + V(r) + \gamma^0 S(r) , \tag{25}$$

m is the free nucleon mass, γ^0 and $\boldsymbol{\gamma}$ are Dirac matrices. The scalar field $S(r)$ consists of the isoscalar and isovector parts resulting from the exchange by σ and δ mesons. In addition to the isoscalar and isovector parts resulting from the exchange by ω and ρ mesons the vector field $V(r)$ includes the Coulomb potential. The small isovector quantity $\Phi(r)$ results from the tensor part of the ρ meson-nucleon coupling. The details of the calculations are described in Ref.[10]. They also may be found in the extensive literature on the Walecka model [12], see for instance Ref.[14].

The Dirac equation $H_{sp}\psi_\lambda = \varepsilon_\lambda\psi_\lambda$ is equivalent to Schrödinger-like one for a particle with the effective mass

$$M(r) \ = \ m + \frac{1}{2}\Big(S(r) - V(r)\Big) \tag{26}$$

in the central

$$U(r) \ = \ V(r) + S(r) \tag{27}$$

and spin-orbit potentials [15]

$$U_{\ell s} \ = \ \frac{1}{r}\ \frac{d}{dc}\left(\frac{1}{2M(r)}\right)\ \boldsymbol{\ell\sigma} . \tag{28}$$

The terms arising from the quantity $\Phi(r)$ are omitted here, but actually they are taken into account in the calculations. The quantities in Eqs.(24)–(28) should be supplied by the subscript "pair" since they describe the contribution from the two-particle forces.

The contribution from the many-particle forces is looked for as the following expansion in terms of the nucleon density distribution $\rho(r)$

$$U_m(r) \;=\; \hbar c \left[a_3 \rho^2(r) + a_4 \rho^3(r) + \;\cdots \right] \tag{29}$$

the ρ^2 term results from three-particle forces, Fig.3a, the ρ^3 one is of four-particle origin, Fig.3b, etc. (the linear density terms enter the two-particle contribution, Eq.(27)). The potential $U_m(r)$ is assumed to be equally distributed between the scalar and vector fields,

$$S_m(r) \;=\; V_m(r) \;=\; \frac{1}{2}\, U_m(r) \;. \tag{30}$$

The only motivation for this assumption is the aim to have as little free parameters as possible.

3.2 Single-particle energies

As mentioned in Sect.2 the single-particle energies may be determined from experiment by using the sum rules (3a)–(5a). The most suitable situation is that for the cases when the absolute value of the single-particle energy ε_λ exceeds the width σ_λ of the distribution region. In these cases all states, over which the single-particle one is distributed, belong to the same nucleus, and therefore the sum rules (3a)–(5a) are saturated by only one term in the lhs, the first for the hole states and the second for the particle ones. Such situation occurs for the peaks in the cross sections of quasielastic knockout reactions $(p, 2p)$ and (p, pn) [16] leading to the hole states with

$$|\varepsilon_\lambda| \;>\; \sigma_{ax} \;\cong\; 20 \text{ MeV} \;. \tag{31}$$

Indeed, according to Eq.(8) the width σ_λ depends on the single-particle wave function ψ_λ rather than the energy ε_λ, thus being roughly the same for all single-particle states. So it is reasonable to identify σ with the largest observed value $\sigma_{\max} \cong 20$ MeV. The latter is the width of the peaks corresponding to the $1s_{1/2}$ hole states. For these reasons the average energies of the above peaks obeying the Eq.(31) condition may be identified with the single-particle energies within the experimental accuracy of $2 \div 3$ MeV. In this way we demonstrated that the Ref.[2] approach permits the model-independent determination of the single-particle energies. It is worth mentioning that the experimental data for the *sp* energies are independent of those for the two-particle contribution to the *sp* potential.

We used the facts that the cross section of the quasielastic knockout reaction leading to the fixed nuclear state is proportional to the spectroscopic factor of this state, and the absolute values of the *s*-factors are not necessary when all states, over which the single-particle one is distributed, belong to the same nucleus (in this case the relative values are sufficient). This is however not the case for weakly bound single-particle states with $|\varepsilon_\lambda| < \sigma_{\max}$. Such states are distributed over actual ones of both $A-1$ and $A+1$ nuclei, and therefore the *s*-factors from both the pickup and stripping reactions are necessary. But the *s*-factors are determined with a rather low accuracy because of both experimental and theoretical ambiguities, and therefore it is unclear how to pin together the *s*-factors from

the two reactions. For these reasons the energies of weakly bound single-particle states are yet unknown. One should also bear in mind that the low-lying states of $A \pm 1$ nuclei forming the Fermi-surface of the closed-shell nucleus A are Landau–Migdal quasiparticles [4] rather than the single-particle states of nucleon. Indeed, the correlation term $\Sigma(x, x'; \varepsilon)$ is included in the quasiparticle energies in contrast to the single-particle ones, see Ref.[4] for details.

3.3 Many-particle forces and specified density distributions

The observed energies of neutron and proton single-particle states in ^{90}Zr are plotted in Fig.4 together with the results of the calculations. As seen from the figure the lowest "pair" states $1s_{1/2}$ are significantly underbound whereas the higher states, especially the $2s_{1/2}$ ones, are overbound. The same compression of "pair" single-particle states occurs in ^{208}Pb, Fig.5, where this effect is even more pronounced, and also in ^{40}Ca, Fig.6. This means that the potential well, including two-particle forces only, is somewhat too wide but insufficiently deep. The isoscalar potentials in ^{90}Zr, "pair", actual and the many-particle contribution, are plotted in Fig.7. As seen from the figure, the many-particle contribution (i.e. the difference between the actual and "pair" wells) consists of the repulsive and attractive parts, the radius of the latter being less than that of the former. So the expansion (29) has to contain at least two terms of different sign obeying the above condition. The most simple possibility is provided by the sum of the three-particle repulsion, $a_3 > 0$, and the four-particle attraction, $a_4 < 0$. Of course we cannot guarantee the absence of contributions from higher many-particle forces. It only should be mentioned that the above possibility corresponds to the least number of free parameters.

Taking into account the possible contribution of many-particle forces to the isovector nuclear potential the quantity $U_m(r)$ is chosen as

$$\begin{aligned} U_m(r) &= \hbar c \Big\{ a_3 \rho^2(r) + a_4 \rho^3(r) - \tau_3 \left[a_3^- \rho(r) + a_4^- \rho^2(r) \right] \rho^-(r) \Big\} , \\ \rho(r) &= \rho_n(r) + \rho_p(r) , \quad \rho^-(r) = \rho_n(r) - \rho_p(r) . \end{aligned} \tag{32}$$

$\rho_n(r)$ and $\rho_p(r)$ are neutron and proton density distributions in nucleus. As seen from Fig.4 the description of single-particle energies is improved by including the many-particle contribution.

The results, which are labelled as "tot" in Fig.4, are obtained using the Woods–Saxon-like density distributions of Ref.[11] which are folded with the nucleon electromagnetic form factor, see Ref.[11] for details. However the nuclear potential is expressed through the point densities since the finite size of nucleon is taken into account in the NN forces. For this reason we used the point densities $\rho_0 W_A(r)$ which are obtained from those of Ref.[11] by usual deconvolution procedure.

It should be mentioned that the electron and proton elastic scattering data underlying these densities are sensitive to nucleon density distributions in the surface region of nucleus, whereas the single-particle energies are sensitive to those in nuclear interior. Therefore the observed single-particle energies may be used to specify the nucleon density

Table 1: Neutron and proton density parameters

	α_n	β_n	α_p	β_p
^{90}Zr	-0.0836	0.4823	-0.0287	0.4416
^{40}Ca	-0.0513	0.5469	-0.0215	0.4557
^{208}Pb	-0.2146	0.4670	-0.0092	0.2200
	-0.3083	0.4646	-0.1308	0.2779

distributions. We tried many different forms of $\rho(r)$. The most appropriate one is found to be

$$\rho(r) \;=\; \rho_0\Big(W_A(r) + \alpha W_A(0)\varphi_4(\beta r)\Big)\;, \tag{33}$$

where $\varphi_4(x)$ is the fourth order Hermite function. The best fit parameters α and β of neutron and proton density distributions are shown in Table 1. The best fit strength parameters are found to be the same for all nuclei. They are

$$\begin{aligned} a_3 &= 13.6608 \text{ fm}^5\;, \quad a_4 = -80.2568 \text{ fm}^8 \\ a_3^- &= 28.7531 \text{ fm}^5\;, \quad a_4^- = -144.3534 \text{ fm}^8\;. \end{aligned} \tag{34}$$

The calculations with the specified densities are labelled as "tot1" in Figs. 4–6.

Slightly better agreement for ^{208}Pb is provided by the following strength parameters

$$\begin{aligned} a_3 &= 15.1120 \text{ fm}^5, \quad a_4 = -90.9870 \text{ fm}^8\;, \\ a_3^- &= 21.0000 \text{ fm}^5, \quad a_4^- = -99.0890 \text{ fm}^8 \end{aligned} \tag{35}$$

with the following form of the nucleon density distributions

$$\rho(r) \;=\; \rho_0 W_A(r)\,(1 + \alpha\varphi_4(\beta r))\;. \tag{36}$$

The corresponding parameters α and β are those of the fourth row in Table 1, the results are labelled as "tot2" in Fig.5.

The largest discrepancy between the observed single-particle energies and the "tot1" results for ^{90}Zr and ^{40}Ca as well as the "tot2" ones for ^{208}Pb is less than 3 MeV, the average discrepancy is 1.65 MeV.

The specified nucleon density distributions are plotted in Figs.8 and 9. As seen from the figures the neutron densities have a pronounced dip in the center of nucleus which increases with increasing mass number.

We also calculated the 1 GeV proton elastic scattering cross sections within the Glauber–Sitenko theory [17] using both the specified densities and those of Ref.[11]. The results, see Fig.10, clearly show that the agreement with experiment is equally good for both the Ref.[11] and the specified densities.

The possible reasons for the difference between the Eq.(34) and the Eq.(35) strength parameters are as follows. (i) Expression (32) corresponds to the zero-range forces

$$f_3(r_{12}, r_{13}) \;=\; (a_3 + \boldsymbol{\tau}_1\boldsymbol{\tau}_2 a_3^-)\delta(r_{12})\delta(r_{13}) \tag{37}$$

$$f_4(r_{12}, r_{13}, r_{14}) \;=\; (a_4 + \boldsymbol{\tau}_1\boldsymbol{\tau}_2 a_4^-)\delta(r_{12})\delta(r_{13})\delta(r_{14})\ , \tag{38}$$

whereas the actual forces may be of finite range. (ii) The above forces should have been folded with the two-particle density and the three-particle one rather than the products of single-particle densities. (iii) As mentioned above, the contributions from higher many-particle forces may be present.

The difference is however small for the charge-symmetric nuclear matter with the equilibrium density $\rho_{eq} = 0.17$ fm^{-3}. Indeed, as follows from Eqs. (32),(34) and (35) the contributions of three(four)-particle forces to the isoscalar single-particle potentials are

$$U_3 \;=\; \hbar c a_3 \rho_{eq}^2 \;=\; 78\ (86)\ \text{MeV}\ , \tag{39}$$

$$U_4 \;=\; \hbar c a_4 \rho_{eq}^3 \;=\; -78\ (-88)\ \text{MeV}\ . \tag{40}$$

The first values in the rhs correspond to the Eq.(34) parameters whereas those in parentheses refer to the Eq.(35) set. They are not small compared to the "pair" value $U_{\rm pair} = -83$ MeV, see Eqs. (24) and (27). But they nearly compensate each other thus giving rise to the conclusion that the isoscalar part of the nuclear single-particle potential is mainly of the two-particle origin. This conclusion is supported by the fact that according to Eq.(30)

$$S_3 = V_3 = 39\,(43)\ \text{MeV}\ , \quad S_4 = V_4 = -39\,(-44)\ \text{MeV}\ , \tag{41}$$

thus being considerably less than the pair values $S_{\rm pair} = -367$ MeV, $V_{\rm pair} = 284$ MeV, see Eq.(24).

The situation is different for the isovector part of the potential. With $\rho^- = \frac{N-Z}{A}\rho_{eq}$ Eq.(32) gives

$$U_m^- \;=\; \hbar c \left(a_3^- \rho_{eq} + a_4^- \rho_{eq}^2\right) \rho^- \;=\; 24\ \frac{N-Z}{A}\ \text{MeV} \tag{42}$$

for both Eq.(34) and Eq.(35) parameters whereas the "pair" value provided by the Bonn B potential is $U_{\rm pair}^- = 7\frac{N-Z}{A}$MeV, the isovector nuclear potential thus being mainly of many-particle origin. The reason is due to the fact that the two-particle contribution arises from the exchange by isovector mesons ρ and δ which are weakly coupled to nucleon [7].

4 Summary

In this way we demonstrated that the many-particle NN interaction includes at least the three-particle repulsion and the four-particle attraction. This result is restricted because no information is obtained for the many-particle forces which do not contribute to the nuclear single-particle potential. But it provides a very instructive example of the situation where the experimental data on complex nuclei are more appropriate for the fundamental problem than those on few-nucleon systems. Indeed, the latter ones

are described by solving the complicated many-particle quantum mechanical problem including the interaction in all orders of the perturbation theory. On the contrary the single-particle states are solutions of the one-particle problem which is much more simple. In addition the nuclear single-particle potential is expressed through the NN interaction in first order of the perturbation theory, the result thus being visual (see Fig.7).

Besides the above-mentioned A dependence of the strength parameters our results may have the following additional ambiguities.

1. They are essentially based on the choice of the Bonn potential for the two-particle NN forces. The reason for this choice is a very high level of confidence: (a) the physics underlying the Bonn potential is absolutely clear, (b) it contains only one adjustable parameter, (c) the two-nucleon data are described with χ^2/datum=1.9 [18] (according to this reference the Bonn B version we used in the present work is completely equivalent to the full one).

Of course our results may be changed with the progress of the knowledge about the NN interaction. We insist however that the acceptable new-fashioned potential must be of higher level of confidence than the Bonn one. This means that (a) the underlying physics should be as clear as that for the Bonn potential, (b) the number of free parameters may be also only one but the χ^2/datum value should be considerably less or (c) the χ^2/datum value may be the same but no free parameters should be present.

2. In the Ref.[16] experiments the energy of the knocked-out nucleon is only about 100 MeV. This may be insufficient to neglect the final-state inelastic interactions leading to additional excitation of the final nucleus. As a result of such excitations the average energies of the peaks may be shifted from the single-particle energy values because the reaction mechanism is not a pure quasielastic knockout in this case. To get rid of this ambiguity the additional quasielastic knockout $(p, p'N)$ or $(e, e'N)$ experiments are desired in which the energy of the knocked-out nucleon would be about 1 GeV. We hope that our work will stimulate such experiments.

The authors are indebted to Dr. M.B. Zhalov for valuable discussions.

References

[1] R.Schiavilla, V.R.Pandharipande and R.B.Wiringa, Nucl.Phys.A **449** (1986) 219.

[2] M.Baranger, Nucl.Phys.A **149** (1970) 225.

[3] A.A.Abrikosov, L.P.Gor'kov and I.E.Dzyaloshinski, *Methods of quantum field theory in statistical physics*, M.1962.

[4] A.B.Migdal, *Finite Fermi-system theory and properties of atomic nuclei*, M. 1983.

[5] K.Erkelenz, Phys.Reports **13** (1974) 191.

[6] M.Lacombe et al., Phys.Rev.C **21** (1980) 861.

[7] R.Machleidt, K.Holinde and Ch.Elster, Phys.Rep. **149** (1987) 1.

[8] K.Brueckner, J.Gammel and H.Weitzner, Phys.Rev. **110** (1958) 431.

[9] S.G.Kadmenski and P.A.Lukyanovich, J.Nucl.Phys. **49** (1989) 1295.

[10] B.L.Birbrair, PNPI Preprint TH-20-1998, No.2234 (1998).

[11] G.D.Alkhazov et al., Nucl.Phys.A **381** (1982) 430.

[12] J.D.Walecka, Annals of Phys.(NY) **83** (1974) 491.

[13] S.J.Wallace, Comments on Nucl.and Part.Phys. **13** (1984) 27.

[14] K.Rutz et al., Nucl.Phys.A **634** (1998) 67.

[15] B.L.Birbrair, L.N.Savushkin and V.N.Fomenko, J.Nucl.Phys. **35** (1982) 1134.

[16] A.A.Vorobyov et al., J.Nucl.Phys. **58** (1995) 1923.

[17] R.J.Glauber, *Lectures in theoretical physics*, ed. W.E.Brittin et al., vol.1 (NY 1959) p.315.

[18] R.Machleight, Adv.in Nucl.Phys. **19** (1989) 189.

Figure Captions

Fig.1. Two-particle (a), three-particle (b), four-particle (c) and higher (d) nucleon-nucleon interaction forces. The wavy lines are for mesons, the full ones are for nucleons.

Fig.2. First-order Hartree (a) and exchange (b) diagrams.

Fig.3. Contributions of three-particle (a) and four-particle (b) forces to nuclear single-particle potential.

Fig.4. Single-particle energies of neutron and proton states in ^{90}Zr. The energy scale is shown from the left of each figure. The labels are " exp " for the observed energies, "pair" for the calculations taking into account the two-particle forces only, "tot" for those including the many-particle forces and using the density distributions from Ref.[11], and "tot 1" for the case when both the many-particle forces and specified densities are included.

Fig.5. The same for ^{208}Pb. The label "tot 2" is for the case when the individual strength parameters for ^{208}Pb are used.

Fig.6. The same for ^{40}Ca.

Fig.7. Isoscalar potential in ^{90}Zr. The full, dashed and dot-dashed lines are for actual, "pair" and many-particle part of the potential respectively.

Fig.8. Neutron density distributions in ^{40}Ca, ^{90}Zr and ^{208}Pb.

Fig.9. The same for protons.

Fig.10. Elastic scattering of 1 GeV protons on ^{40}Ca, ^{90}Zr and ^{208}Pb. The calculations with the specified densities are shown by full line, those with the Woods–Saxon-like ones from Ref.[11] are plotted by dashed line, the dots are for the experimental data.

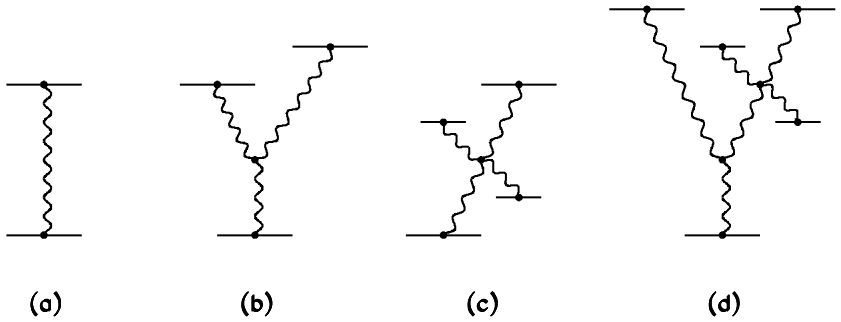

Fig.1

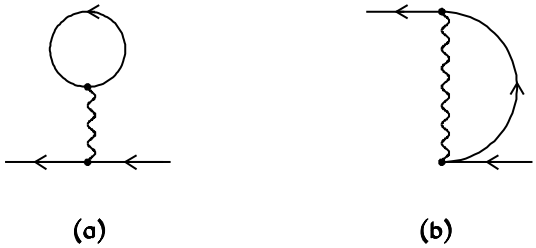

Fig.2

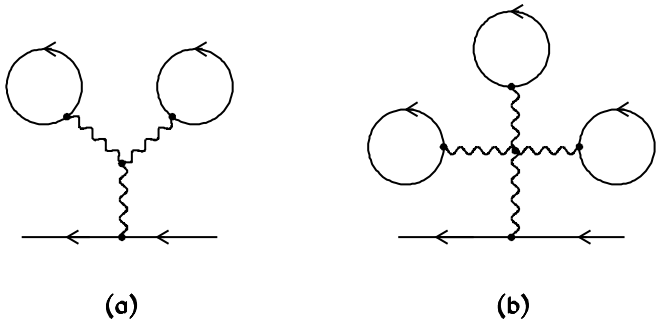

Fig.3

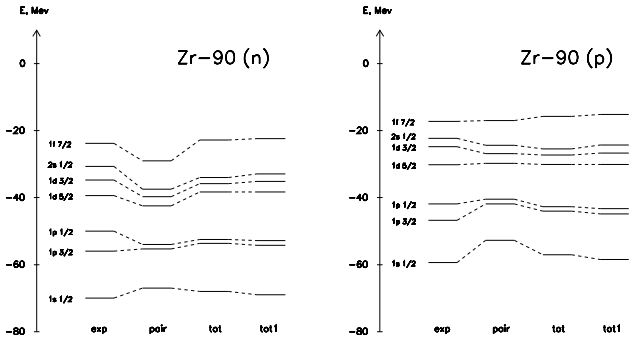

Fig.4

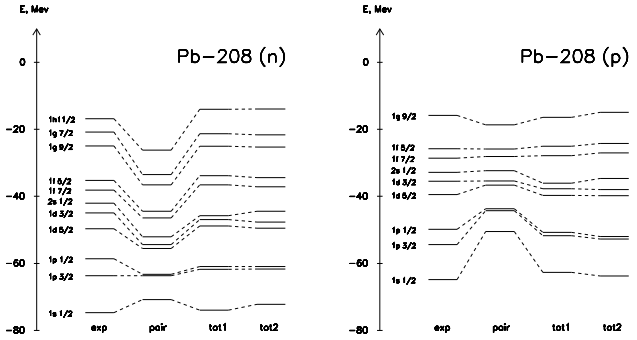

Fig.5

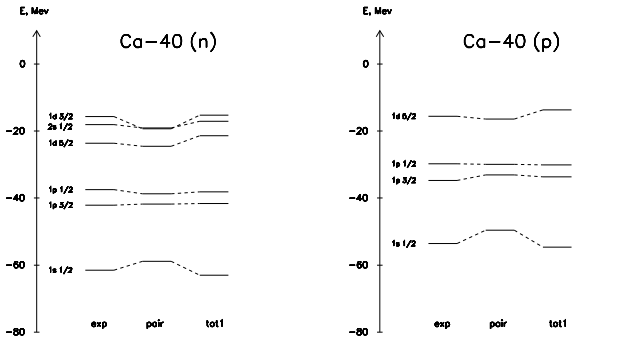

Fig.6

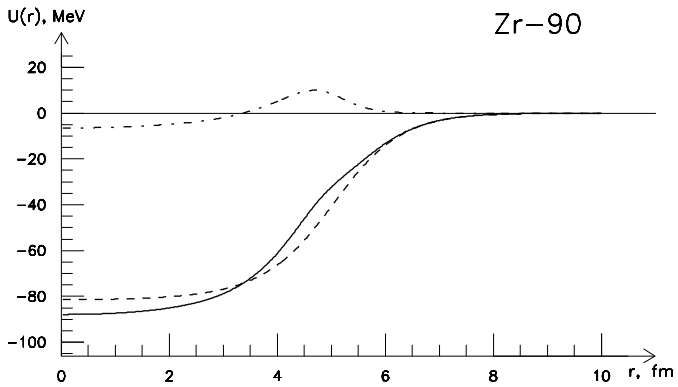

Fig.7

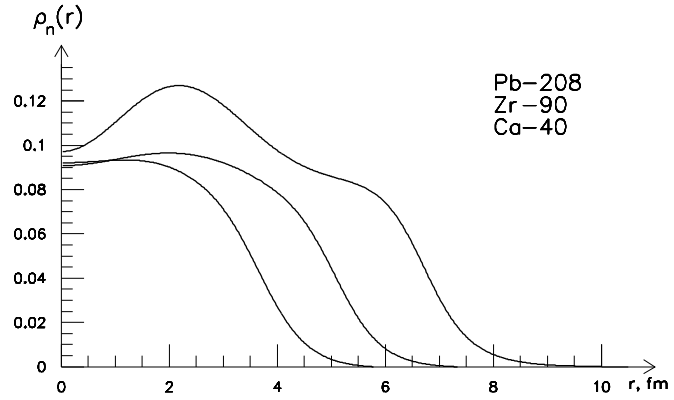

Fig.8

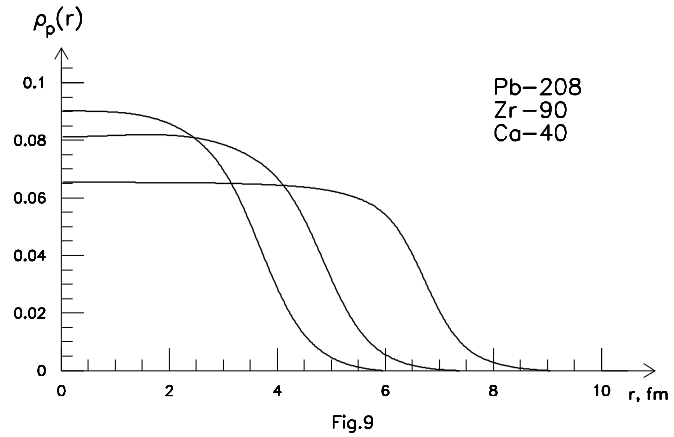

Fig.9

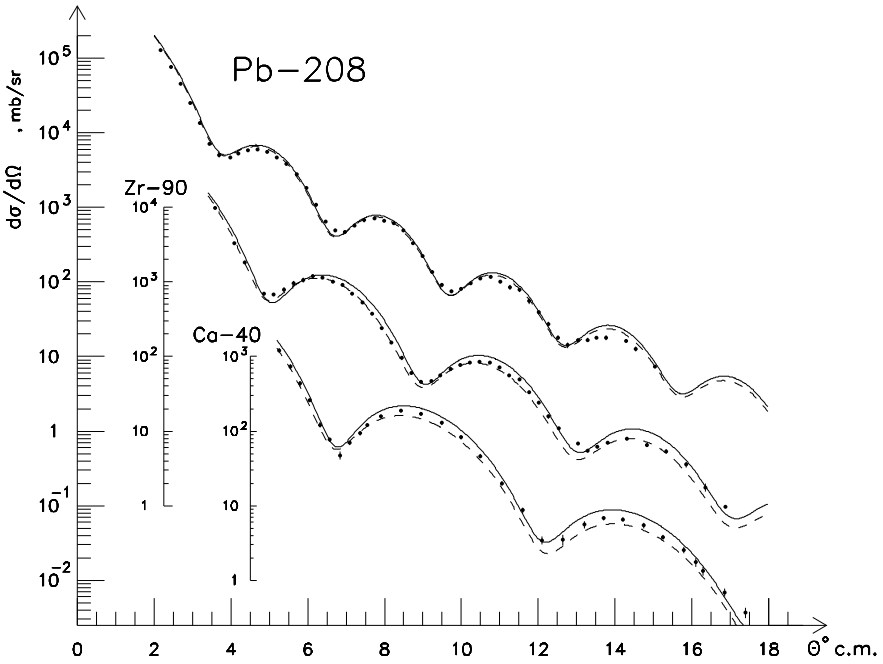

Fig.10